Final Results for Photobit Active Pixel Sensor Heavy-Ion Transient Response Test

Cheryl J. Marshall, Kenneth A. LaBel, Robert A. Reed
Code 561
NASA Goddard Space Flight Center
Greenbelt, MD 20771 USA
cmarshall2@aol.com

Paul W. Marshall
NASA Consultant
7655 Hat Creek Road, Brookneal, VA 24528 USA

Wheaton B. Byers, Christopher Conger, Joe Peden
Scientific Applications International Corporation (SAIC)
McLean, VA 22102 USA

El-Sayed Eid
Gentex Corporation
600 N. Centennial St., Zeeland, MI 49464 USA

Michael R. Jones, Scott Kniffin
Orbital Sciences Corporation
Greenbelt, MD 20771 USA

George Gee
Stinger Ghaffarian Technologies, Incorporated
Greenbelt, MD 20771 USA

Jim Pickel
PR & T, Inc.
Fallbrook, CA 92028 USA

DUT: Experimental rad-hardened Photobit Active Pixel Sensor (tested @ room temperature)
Date: 27 March 2001
Facility: Texas A&M University (TAMU) Cyclotron Facility
Ion: Argon at 15 MeV/amu (LET=8.44 MeV-cm^2/mg @ normal incidence)

1. Introduction

The Photobit 256x256 format imager is segmented into four quadrants. Individual quadrants have been fabricated with different experimental processing techniques. The objective is to evaluate the transient behavior of the imager in response to heavy-ion ionization events. the physical design techniques of enclosed geometry and p-channel guard rings is used to design and lay out a set of four N-type radiation tolerant active

photodiode (PD) pixels. The sensor arrays are standard 0.35 μm CMOS technology fabricated with a mixed mode, twin well process with 7.0 nm gate oxides. The 256 x 256 full array has four sub arrays (or quadrants) made up of 16.2 μm by 16.2 μm pixels. The key design features of the test chip are summarized in Table 1.Variations in the behavior of the quadrants could provide guidance regarding the correct direction to take in the development of an APS imager suitable for space applications.

We have reduced the 15 MeV/amu Argon data series obtained at Texas A&M University cyclotron facility in College Station, TX (TAMU). Measurements were made using ^{40}Ar at 15.0 MeV/amu, ^{84}Kr at 15.3 MeV/amu, and ^{131}Xe at 15.2 MeV/amu. Data has been taken at three angles of incidence: normal, 60º from normal and 75º from normal. The azimuth angle was not varied. Each test sequence consists of 100 full frames of data acquired by reading the imager out continuously during exposure. A typical data set starts with ~10 dark frames before exposure to the ion beam begins. When 70-80 frames of ion data have been acquired the beam is turned off. The remainder of the 100 frame group is completed with a second series of dark images.

2. Data Processing

The data was originally distributed in 100 frame movie sequences taken at 0º, 60º and 75º packed in three separate files. Individual frames were extracted and rewritten in Flexible Image Transport (FITS) format. Subsequent manipulation and analysis of the data was performed on the converted FITS images.

Dark subtraction was executed using super-dark frames generated separately for each test sequence (3 different super-darks for the 3 angles of incidence). A super-dark was created by combining all of the darks preceding and following the exposure, typically ~20 frames total. Every pixel of the super-dark is the median of the signal contained in the corresponding pixel of the individual frames.

All data frames were super-dark subtracted before analysis. We found that the elimination of spatial noise due to non-uniformities in dark current resulted in a significant decease in the background noise floor by a factor of ~5-10. Faint diagonal striping (‘herring-bone’) was observed in the data frames after super-dark subtraction. We did not attempt to remove this residual pattern noise.

The background signal in the data images was not completely removed by dark current subtraction. A small amount of background signal, typically averaging ~5-15 counts, persisted in all of the data frames. We do not yet understand the cause of this residual signal.

We analyzed the tracks in the exposed frames by manually sampling and extracting hundreds of individual ion strikes from the images. An Interactive Data Language (IDL) software package was developed to facilitate this process. The software incorporates a graphical front end with visual tools that allow the user to interactively build a database of measurements by selecting from the images individual ion tracks that are well isolated from surrounding ion tracks.

Every ionization event selected for the database was sampled with a rectangular window centered on the first-moment centroid of the ion track. The dimensions of the rectangular window were varied for each quadrant and angle of incidence. We tried to achieve the best balance between database size (the number of individually sampled ion strikes) and capture of signal due to the spread of charge away from the ion track.

The sensitivity of the imager to ionization was quantified by measuring the total detected signal contained within the track. This is the simple sum of the signal contained in every pixel within the rectangular sampling window. Random noise in background pixels not containing charge from the ion will approximately cancel if the residual signal remaining after dark current subtraction is removed.

We evaluated the area of charge spread by measuring the number of pixels containing detectable charge deposited by the ion ('disturbed' pixels). The measurement was performed by counting all pixels within the sample window containing positive signal in excess of 3s of the background noise floor. Like the total signal measurement, this method of counting disturbed pixels requires removal of the residual background signal in the dark subtracted images.

For the total signal and disturbed pixels measurements, we used the perimeter pixels of the sampling window to obtain a local estimate of the background offset. We experimented with three different simple methods of background offset removal to assess the sensitivity of the results to the choice of algorithm. The initial measurements were repeated with the background offset determined from the mean, the median and the two-pass mean (3s rejection of outliers after the first mean) of the signal in the perimeter pixels. We found the results to be essentially insensitive to the offset removal approach, although a slight systematic difference was noted between the median and the two different mean methods. The final data set was measured with the two-pass mean background estimator.

We reduced the Argon series twice. The first round of reduction was a learning exercise to simultaneously develop the IDL software package and to evaluate algorithm sensitivities such as sampling window size and background offset estimation. Final data reduction exploited lessons learned from the first round.

3. Reference System

We have established a numbering scheme for identification of the four quadrants of the active pixel sensor. Figure 1 shows an example image from the normal incidence Argon sequence. Quadrants 2 and 4 (Q2 and Q4) reference the segments of the APS on the right side of the image. These quadrants visually exhibit the greatest sensitivity to the ion strikes. The mildest response appears visually to occur in Quadrant 3 (Q3), the lower left segment of the frame.

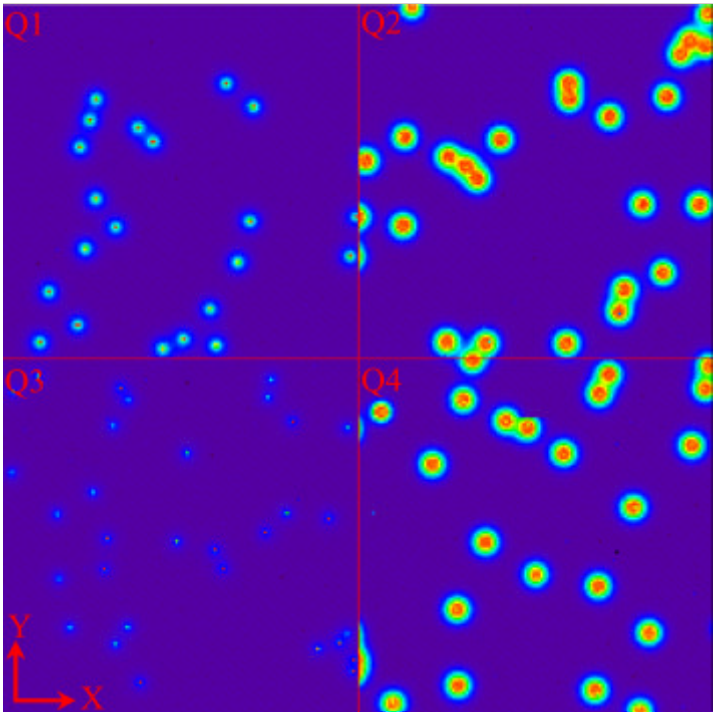

Figure 1. Reference system.

Quadrant boundaries are delineated in Figure 1 by the horizontal and vertical lines superimposed on the image. In data processing we utilize a zero-indexed X-Y coordinate system having an origin coinciding with the pixel at the lower left corner of Q3.

4. Data Set Summary

Table 1 summarizes the database for each quadrant and angle of incidence for the final round of data reduction.

Quadrant	Angle of Incidence	Number of Sampled Hits	Window Size (pixels)
Q1	0º	179	23x23
Q1	60º	124	31x23
Q1	75º	157	27x24
Q2	0º	106	25x25
Q2	60º	99	31x25
Q2	75º	122	30x25
Q3	0º	273	21x21
Q3	60º	143	35x23
Q3	75º	135	26x20
Q4	0º	106	30x27

Q4	60º	91	33x26
Q4	75º	106	30x27

Table 1. Argon database summary.

Compared to the initial round of data processing, we elected to select fewer hits for the database and sample the hits with a larger window. In first round data reduction we found that the total signal and disturbed pixels measurements are sensitive to the size of the sampling window. Window size has a relatively minor impact on the total signal measurement since the total signal is dominated by charge deposited at the point of impact of the ion. The disturbed pixels measurement is significantly more sensitive to window size because of the faint, extended halo of charge that surrounds the ion track.

5. Total Signal Measurement

Figure 2 shows the final pass results for the total signal measurement. The total detected signal in all four quadrants grows as the angle of incidence increases. This is the result of the longer path length of the ion track at non-normal incidence. Quadrant 3 is the least sensitive to ion ionization, followed by Q1. The sensitivity is greatest for Quadrants 2 and 4 with both quadrants exhibiting almost identical behavior. These trends are consistent with our expectations from qualitative visual comparison of the ion tracks in the images. First round data reduction yielded total signal measurements systematically slightly lower than the final round results by ~5-30%, but the trends between the quadrants and the shapes of the curves were the same.

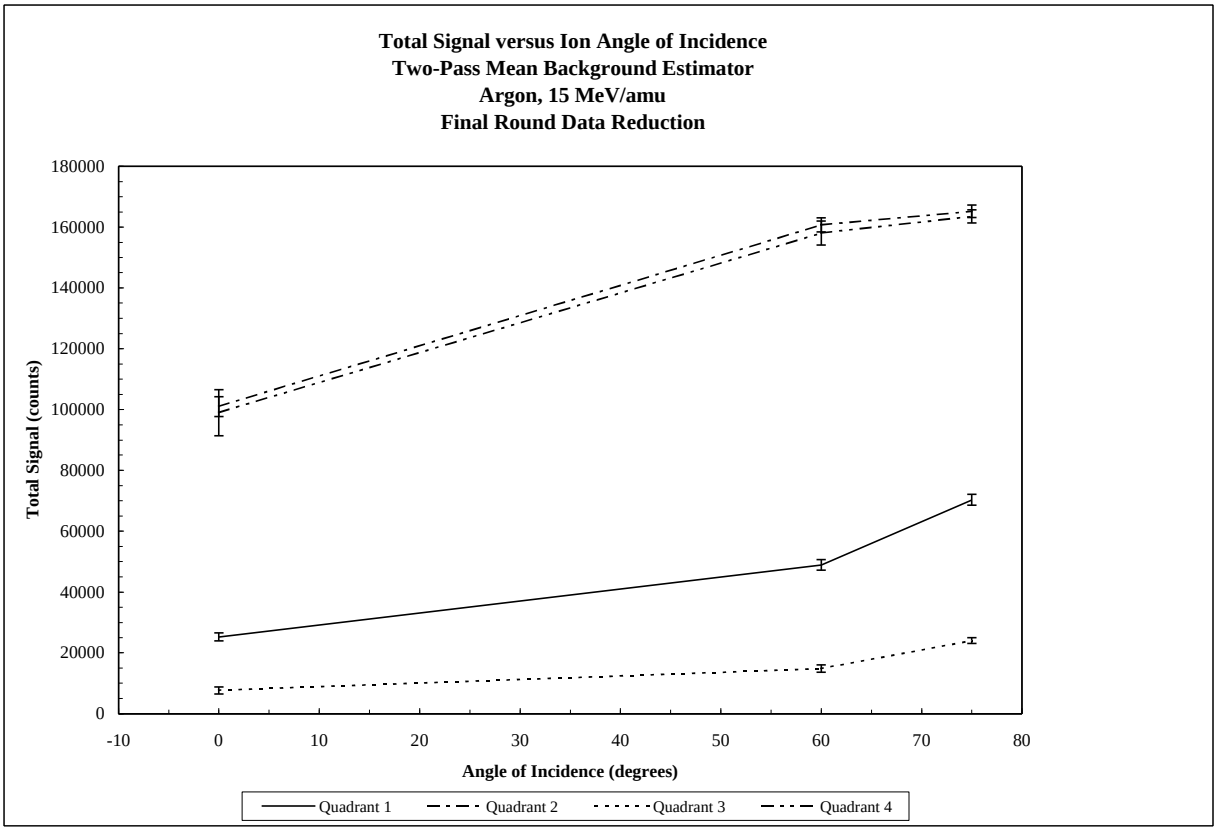

Figure 2. Total signal results.

Total signal measurements for Q2 and Q4 are not accurate representations of the total deposited charge because the pixels at and immediately surrounding the point of impact are full well saturated (see Section 7). The total signal measurement for all quadrants is actually a lower bound since signal below the noise floor will not be detected. Although it varies somewhat from frame to frame because of intermittent pattern noise, the noise floor is typically 5-10 counts rms after dark current subtraction.

We present the total signal measurements (and the ion track contours, see Section 7) in units of raw counts. For rough conversion from signal in counts to charge in electrons we suggest a system gain of 98 electrons/count[1]. The total measured signal therefore ranges from ~7.5e5 electrons (Q3, 0°) to ~1.6e7 electrons (Q2, 75°) with a noise floor that determines the threshold of detection of ~500-1000 electrons rms. The numerical data is summarized in Appendix A.

6. Disturbed Pixels

[1] Derived from the SAIC Photobit SEU/SEL Ion Testing status report dated 27 March, 2001: 488 µV/DN ÷ 5 µV/e^- ˜ 98 e/DN.

The disturbed pixels measurement indicates that a broad halo of diffuse charge spreads away from the track of the ion as it passes through the substrate of the imager. Figure 3 plots the final pass data, which is also tabulated in Appendix B.

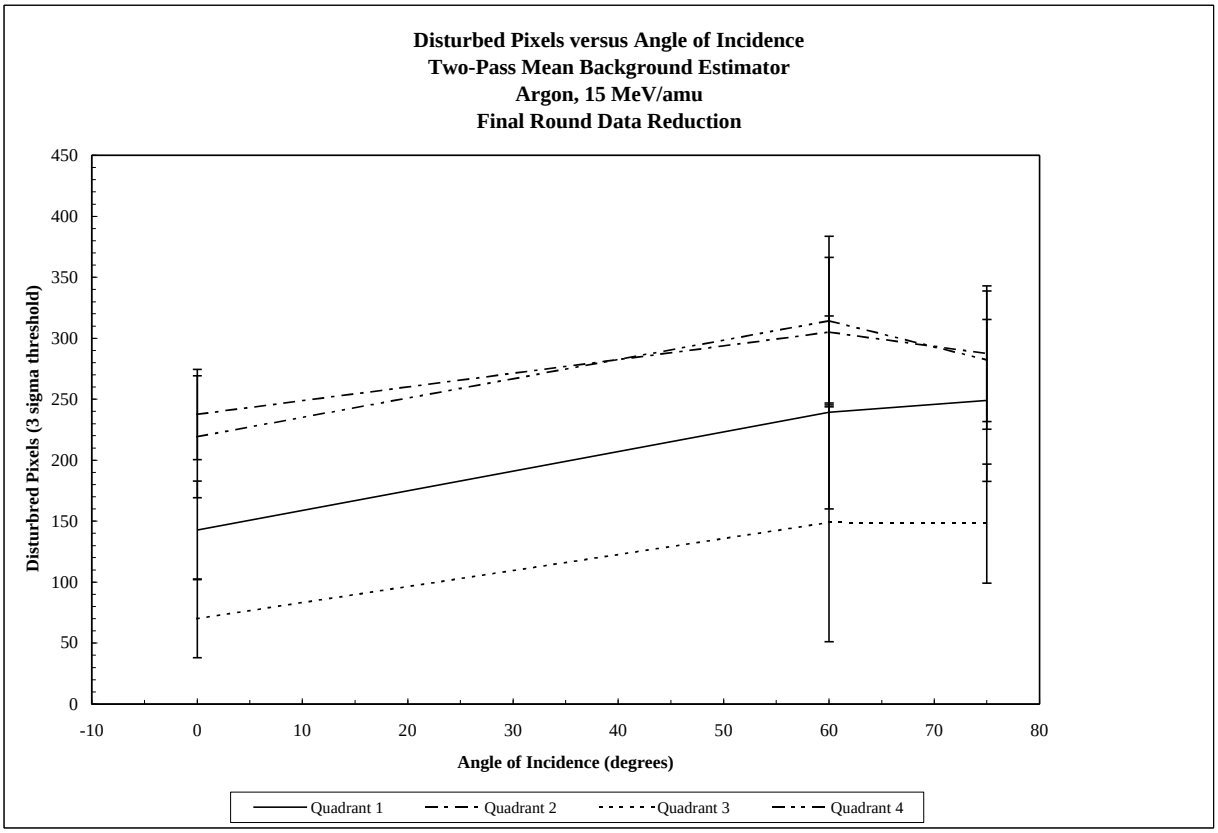

Figure 3. Disturbed pixels results.

Trends exist in the relative ionization responses of the four quadrants that are qualitatively consistent with the total signal measurements. Quadrant 3 exhibits the least amount of charge spread. In the other three quadrants, hundreds of pixels are contaminated by diffusion of charge away from the point of impact. Charge spread in quadrants 2 and 4 is essentially the same and appears to be greater than the charge spread in Q3 by a factor of ~2-3. We note that even for quadrant 3 at normal incidence, an ion strike contaminates 70 pixels on average. The first round results differed substantially; lower by nearly a factor of 3 in the worst case, because of the smaller window size chosen for first round data processing.

The disturbed pixels measurement is a lower bound estimate of the actual number of pixels perturbed by the passage of the ion. Charge contamination is detected by searching for pixels with signal greater than +3s relative to the background noise floor. For the typical noise floor of 5-10 counts rms, the threshold for detection of a disturbed pixel is 15-30 counts (~1500-3000 electrons). The total signal measurements imply that quadrants 2 and 4 more efficiently collect deposited charge than Q3. Differences in charge diffusion in quadrant 3 and quadrants 2 and 4 may not be as great as the factor of

2-3 implied by the disturbed pixels measurements. There could be a significant number of contaminated pixels at the edge of the halo in Q3 that are not detectable above the 3s threshold.

7. Ion Track Morphology

To elucidate the structure of the ionization signature, contours of the ion tracks were generated for each quadrant and angle of incidence. We combined all the individual images in the database to form a final image. Registration of individual images was accomplished by centering the sampling window at the first moment centroid of the ion track. To improve the signal-to-noise of the final images, we used pixel-by-pixel median filtering. We generated a second final image set with simple unweighted pixel-by-pixel averaging for comparison. The background offset was slightly higher in the averaged images, but otherwise the salient features of the ion signature were similar to the median filtered images. Appendices C-F contain the contour data for the four quadrants.

Figure 4 shows an example of the normal incidence ion signature that contrasts the response of the different experimental quadrants of the imager. Signal in the contour plots is in units of counts. Grid intersection points correspond to the centers of pixels. Contour resolution is limited by the noise floor of the median filtered data, which is typically <2 counts (~200 electrons) rms.

Quadrant 3 is clearly the least susceptible to charge contamination from heavy ion ionization. Pixels at and immediately surrounding the point of ion impact in Quadrants 2 and 4 (not shown, but qualitatively similar to Q2) full well saturate. Charge collection in Q3 does not cause saturation. Saturation in Q2 and Q4 occurs at a signal level of ~1700 counts (~170,000 electrons)[2].

Detectable charge diffusion is greatest in Quadrants 2 and 4. The outer edge of the 100-200 count contour extends to a radius of ~7 pixels in Q2 and Q4 whereas in Q3 the =100 count radius is ~2 pixels. For normal incidence, ionization from each ion hit generates =100 counts of signal in Q2 and Q4 over an area roughly 10X larger than in Q3. As expected, the ionization signature is circular symmetric except for a subtle asymmetry visible in some of the contours to the right and below the point of the ion strike. We believe the asymmetry is a test artifact caused by the beam not being exactly perpendicular to the plane of the imager.

Changes in the track signature as a function of incidence angle are illustrated by the sequence in Figure 5. The ions pass through and eventually exit the substrate from left to right. Peak signal occurs at the point of impact at 60º and along a narrow track coinciding with the path of the ion at

[2] Full well for the experimental imager is ~200,000 electrons according to the 27 March, 2001 SAIC Photobit SEU/SEL Ion Testing status report.

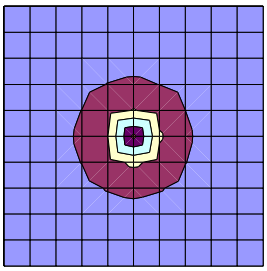

(a)

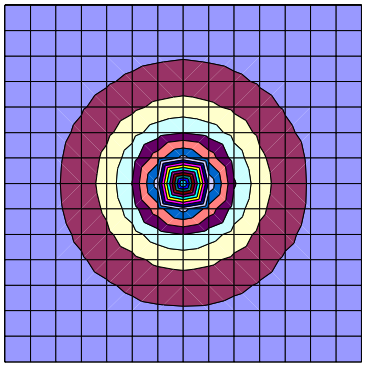

(b)

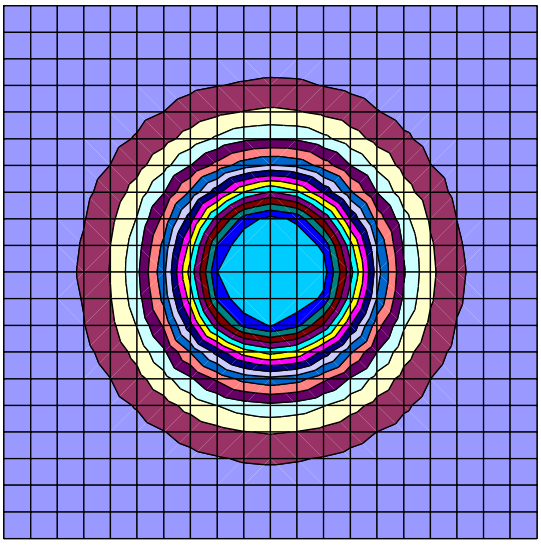

(c)

Figure 4. Normal incidence ionization signature: (a) Q3, (b) Q1, and (c) Q2. Contours are linear with a bin width of 100 counts starting at 0 counts.

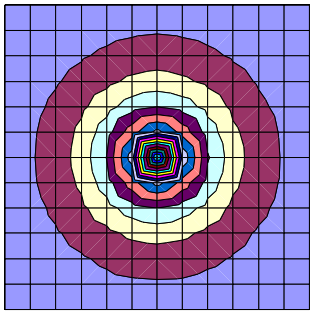

(a)

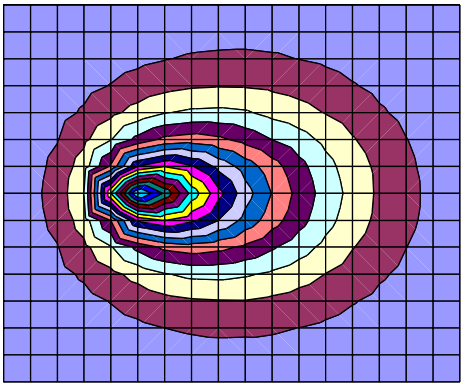

(b)

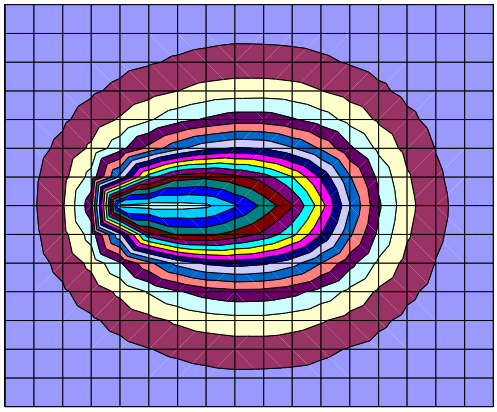

(c)

Figure 5. Quadrant 1 track signature versus angle of incidence: (a) 0º, (b) 60º, and (c) 75º. Contours are linear with a bin width of 100 counts starting at 0 counts.

75º. Evolution of the track signature as a function of angle in Q1 is similar to that of Q3. The circular core of saturated pixels seen in Q2 and Q4 at normal incidence broadens into a swath along the ion path at 60º and 75º. This suggests that the active regions in Q2 and Q4 are relatively deep compared to the active regions in Q1 and Q3.

The oval-shaped signature is the result of recombination, charge collection, diffusion and the increase in path length of the ion through the substrate with increasing incidence angle. At the point of impact, a relatively large fraction of the deposited charge is collected before recombination occurs. Deeper in the substrate, a greater percentage of the deposited charge is lost through recombination. Diffusion in the substrate gives rise to the spread in the signal contours in the X and Y directions.

In an ideal imager with perfect charge collection efficiency and zero charge diffusion, the track length will increase as sec *?*. The measured maximum overall track length increases more slowly than predicted by sec *?* because of charge diffusion away from the point of impact in both directions along the X-axis. The maximum width of the track signature in the Y direction is independent of angle, as expected. We note that even for Q3 the charge spread in the X and Y directions is appreciable at large angles of incidence: the maximum 75º X and Y 100 count contour widths are ~11 pixels and ~7 pixels, respectively (Figure E3, Appendix E). We also find for Q3 that the area contaminated with signal =100 counts relative to normal incidence increases by ~3X at 60º and by ~4X at 75º.

8. Conclusions and Recommendations

Significant differences have been found in the ionization responses of the four quadrants of the experimental sensor. The data shows that the processing utilized for the fabrication of quadrant 3 (see Figure 1 for our reference system) is least sensitive to charge contamination from heavy ions. Compared to Q3, the processing of quadrants 2 and 4 is highly susceptible to ionization. Ion hits in Q2 and Q4 cause saturation of the pixels at the point of impact and charge spread perturbs hundreds of pixels surrounding the ion track. Quadrant 1 has a response characteristic intermediate between the severe charge contamination of quadrants 2 and 4 and the mild response of Q3. Judged strictly from the heavy ion ionization data, the processing of Q3 appears to be best suited for star tracking, scientific imaging and other space-based applications.

We have found that ion track analysis is quite sensitive to the size of the window used to sample the data. Care should be exercised during data reduction to ensure that window dimensions are chosen that yield reliable results.

The background noise floor in the raw images is dominated by dark current non-uniformity. Dark current subtraction is critical for high resolution analysis of ion track morphology. Testing should always include a sufficient number of dark frames to generate a super-dark image.

An unexplained residual background signal exists in the dark current subtracted ion images. It is unclear whether the offset is a radiation effect or an artifact of the test apparatus.

We suspect that the intermittent low-level pattern noise in the dark current subtracted images is a contributing factor to the large uncertainties in the disturbed pixels measurement and to the noise floor in the ion track contour plots. For future work we recommend improved EMI shielding and/or filtering of the electronics and harnesses to reduce or eliminate contamination of the data by pattern noise.

Study of the ionization response at a different LET might be useful for model validation. Data for other ions was obtained during the Texas A&M test run. We suggest reduction of the 0º and 60º Xe-131 data to supplement the Ar track analysis results.

Finally, we note that for LEO missions the primary threat will be protons in the SAA. In Polar LEO, MEO and high altitude orbits the imager will be exposed to a background flux of GCRs and to solar particle events. The GCR composition is mostly hydrogen (protons) with additional minor components of He, Fe and other heavy elements. Solar particle events produce large, transient fluxes of high energy protons. Heavy ion testing is the crucial first step for evaluation of the experimental sensor for spacecraft applications. We argue that proton testing is a necessary and logical next step to predict the performance of the imager in the space radiation environment.

Appendix A

Summary of Total Signal Data

Quadrant	Angle of Incidence	Total Signal (counts)	Total Signal* (electrons)
Q1	0º	25248±1311	2.5e6±1.3e5
Q1	60º	48899±1699	4.8e6±1.7e5
Q1	75º	70324±1775	6.9e6±1.7e5
Q2	0º	101004±3286	9.9e6±3.2e5
Q2	60º	160745±2301	1.6e7±2.2e5
Q2	75º	165206±2052	1.6e7±2.0e5
Q3	0º	7656±1165	7.5e5±1.1e5
Q3	60º	14821±1163	1.4e6±1.1e5
Q3	75º	24010±941	2.3e6±9.2e4
Q4	0º	99005±7532	9.7e6±7.4e5
Q4	60º	158080±3967	1.5e7±3.9e5
Q4	75º	163525±2169	1.6e7±2.1e5

*approximate detected charge for an assumed system gain of 98 e^-/DN

Appendix B

Summary of Disturbed Pixels Data

Quadrant	Angle of Incidence	Disturbed Pixels*
Q1	0º	143±40
Q1	60º	239±79
Q1	75º	249±66
Q2	0º	237±37
Q2	60º	305±61
Q2	75º	287±56
Q3	0º	70±32
Q3	60º	149±98
Q3	75º	148±49
Q4	0º	219±50
Q4	60º	314±69
Q4	75º	282±57

*pixels with signal > 3s above noise floor

Appendix C

Quadrant 1 Ion Track Contours

Median Filtered Image
Argon, 15MeV/amu
Quadrant 1, Normal Incidence
Final Reduction

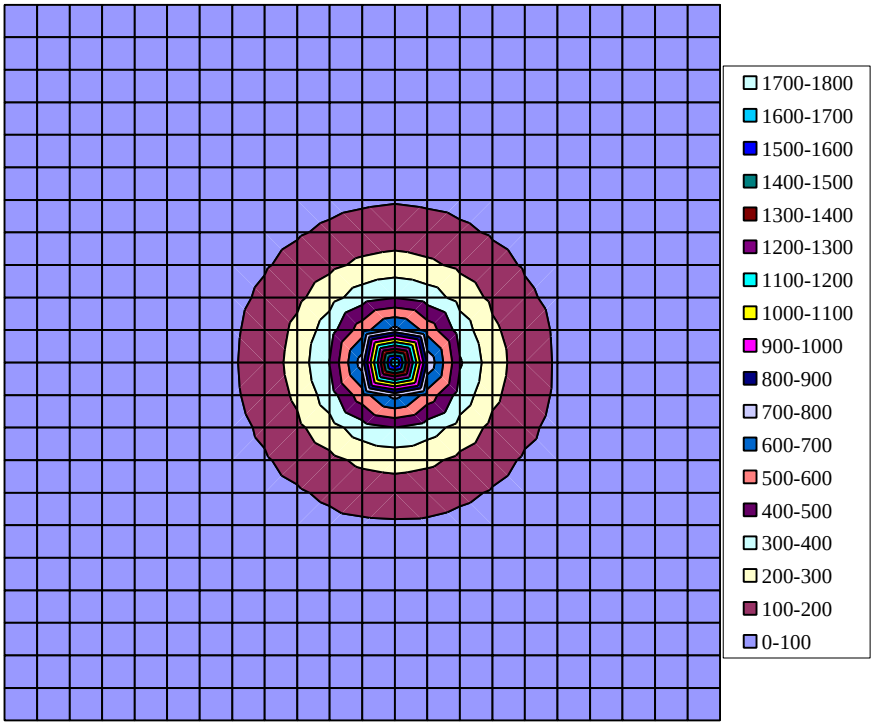

Figure C1. Quadrant 1 0º ion track. Signal is in counts.

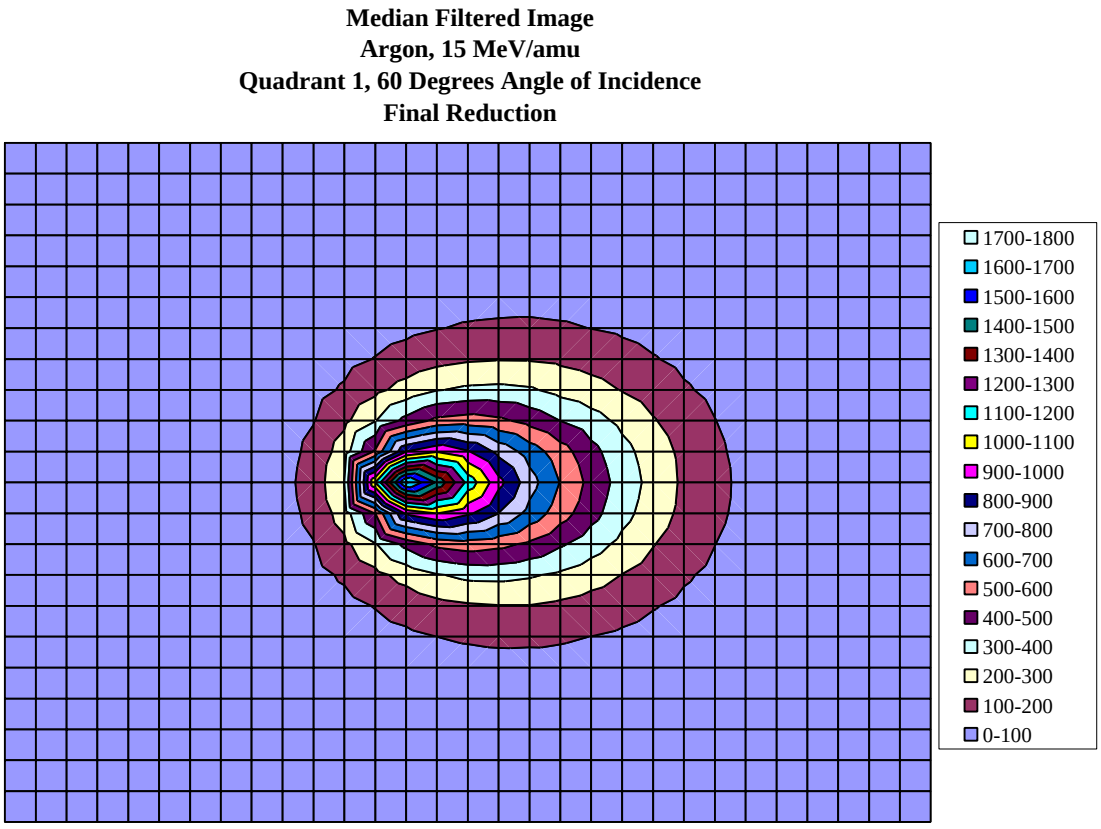

Figure C2. Quadrant 1 60º ion track. Signal is in counts.

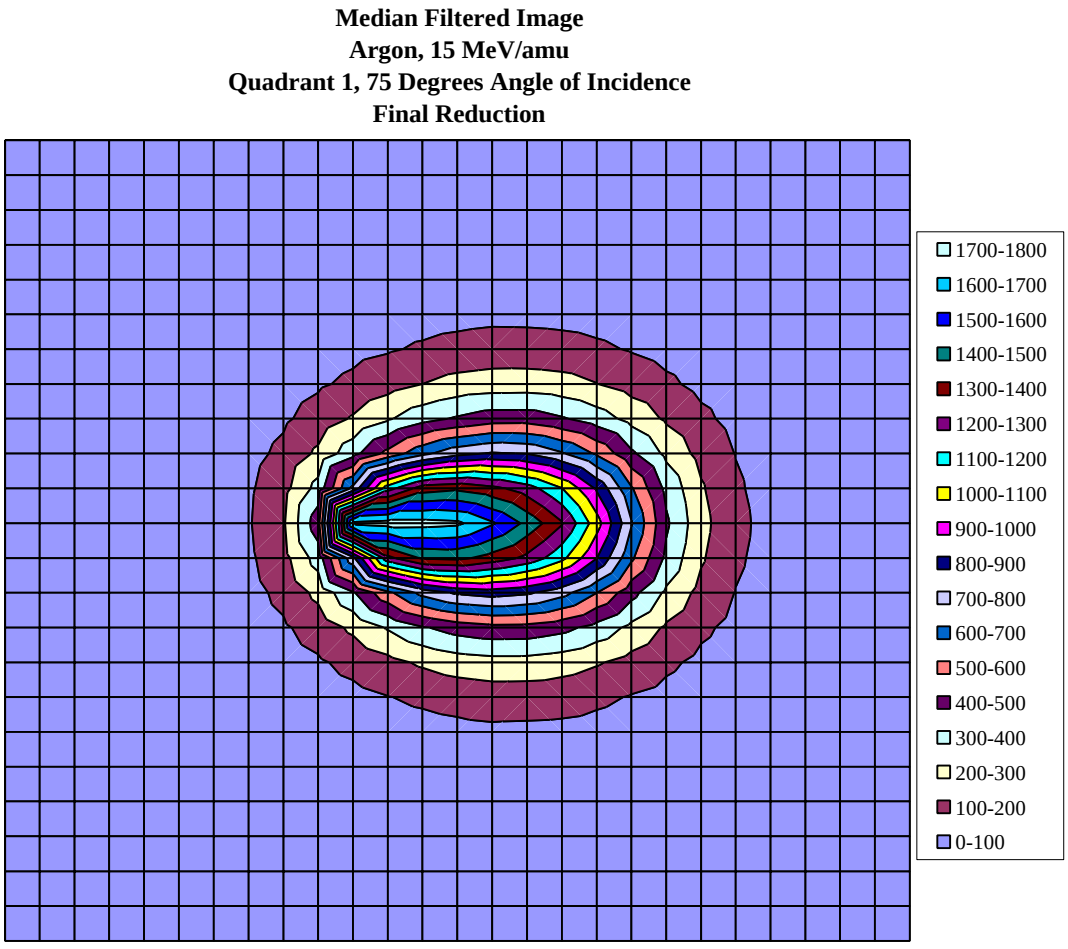

Figure C3. Quadrant 1 75º ion track. Signal is in counts.

Appendix D

Quadrant 2 Ion Track Contours

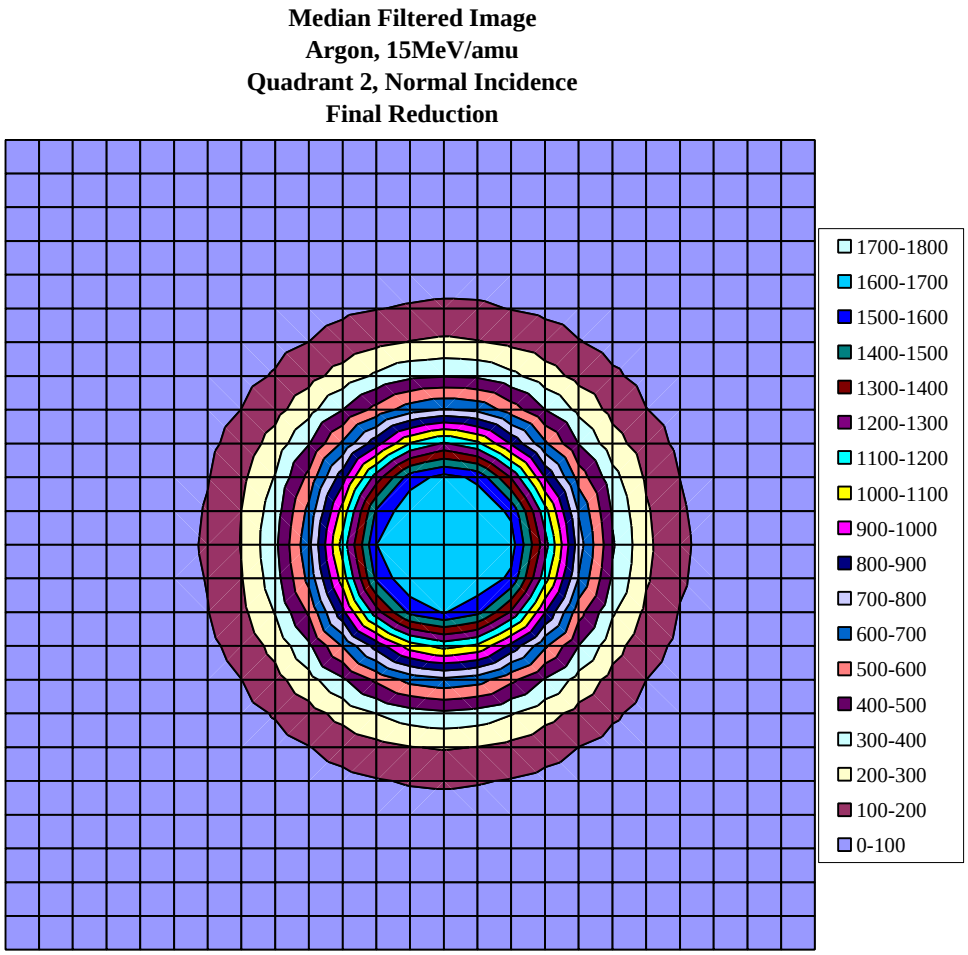

Figure D1. Quadrant 2 0º ion track. Signal is in counts.

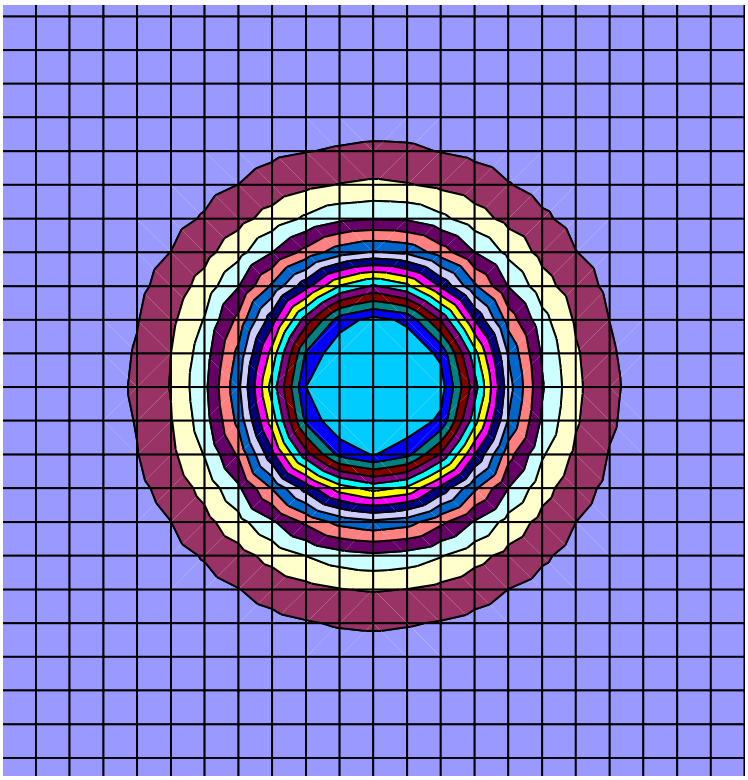

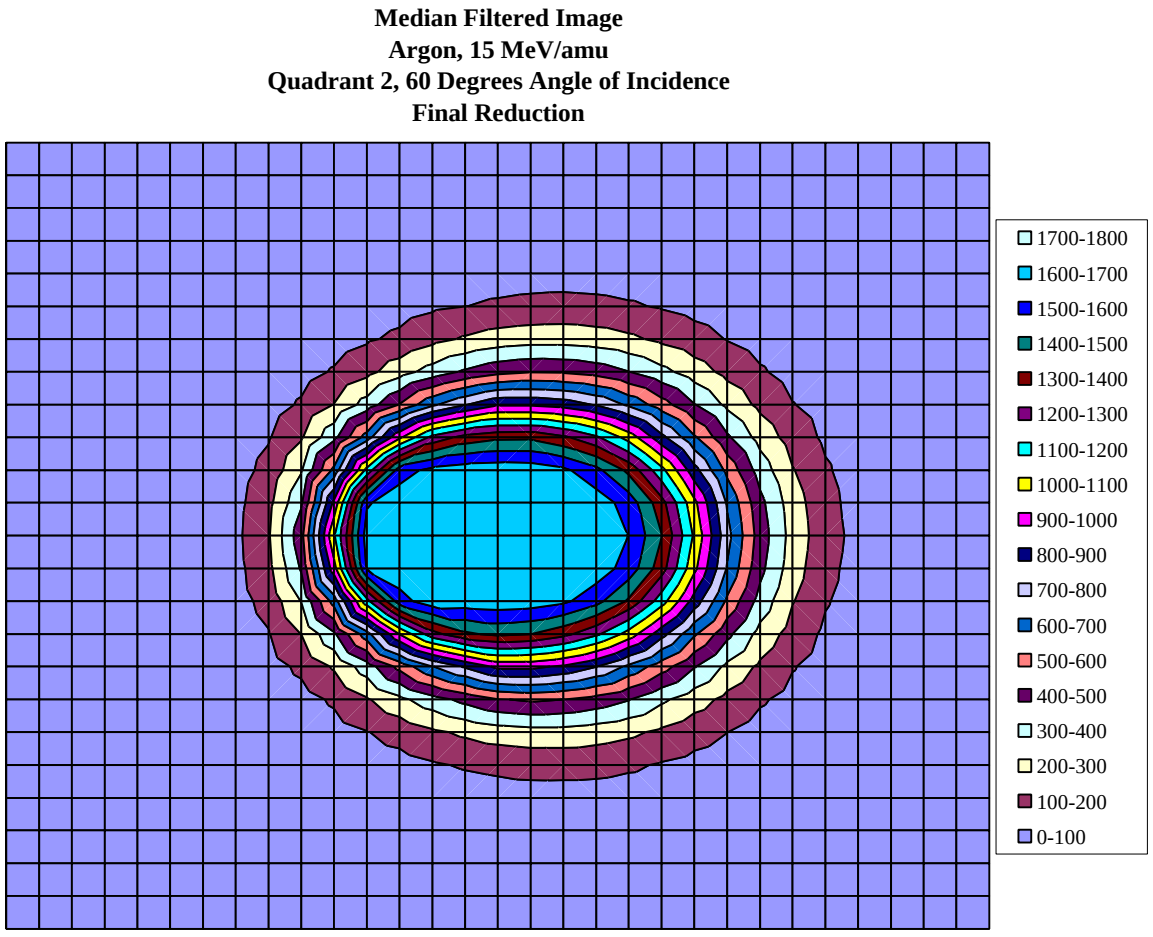

Figure D2. Quadrant 2 60º ion track. Signal is in counts.

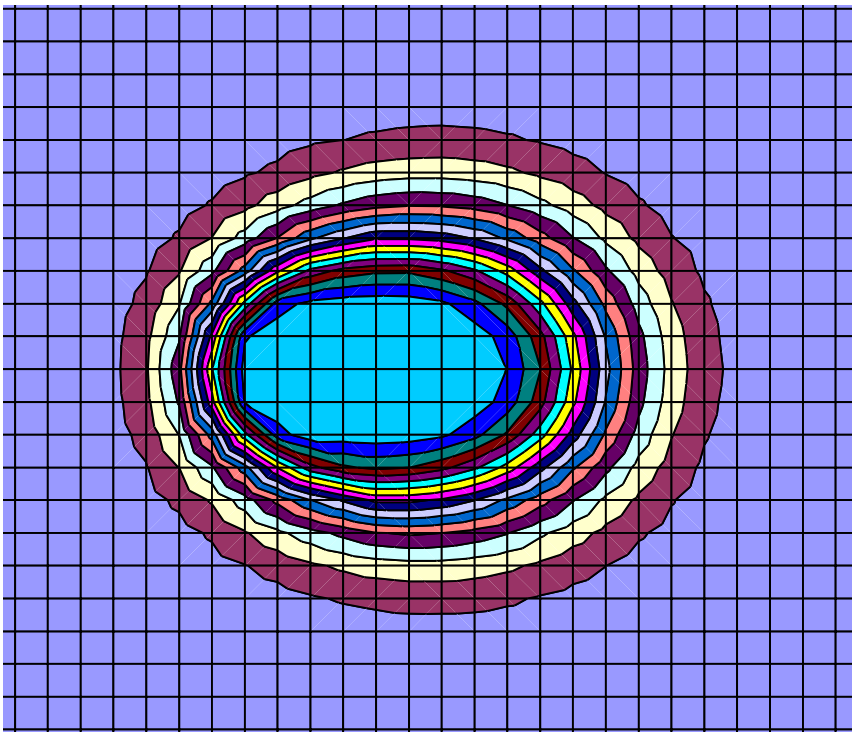

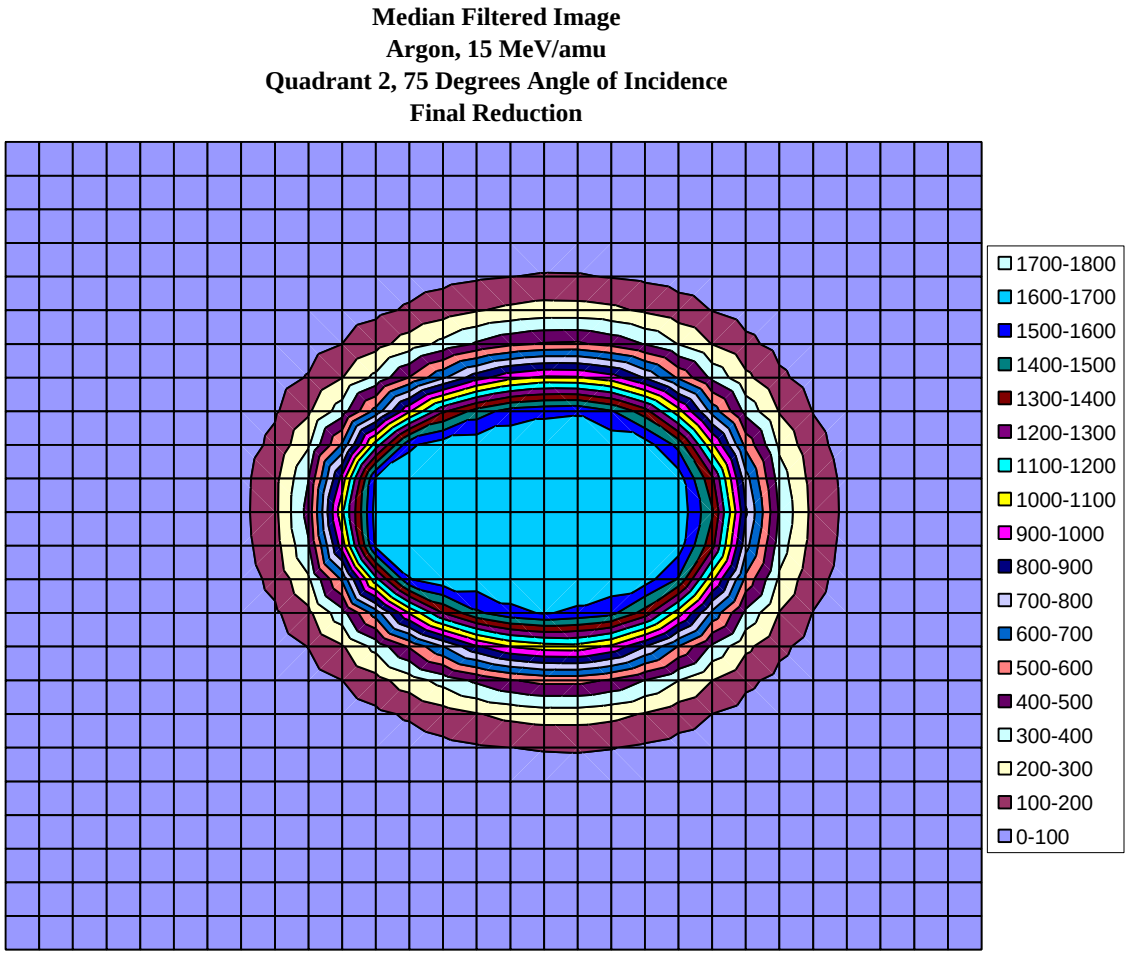

Figure D3. Quadrant 2 75º ion track. Signal is in counts.

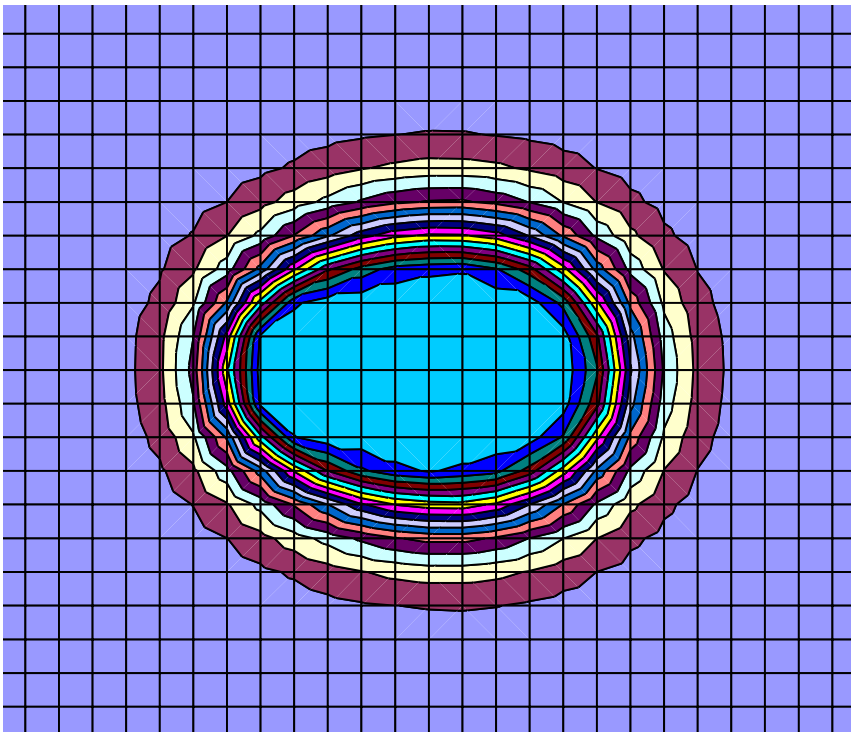

Appendix E

Quadrant 3 Ion Track Contours

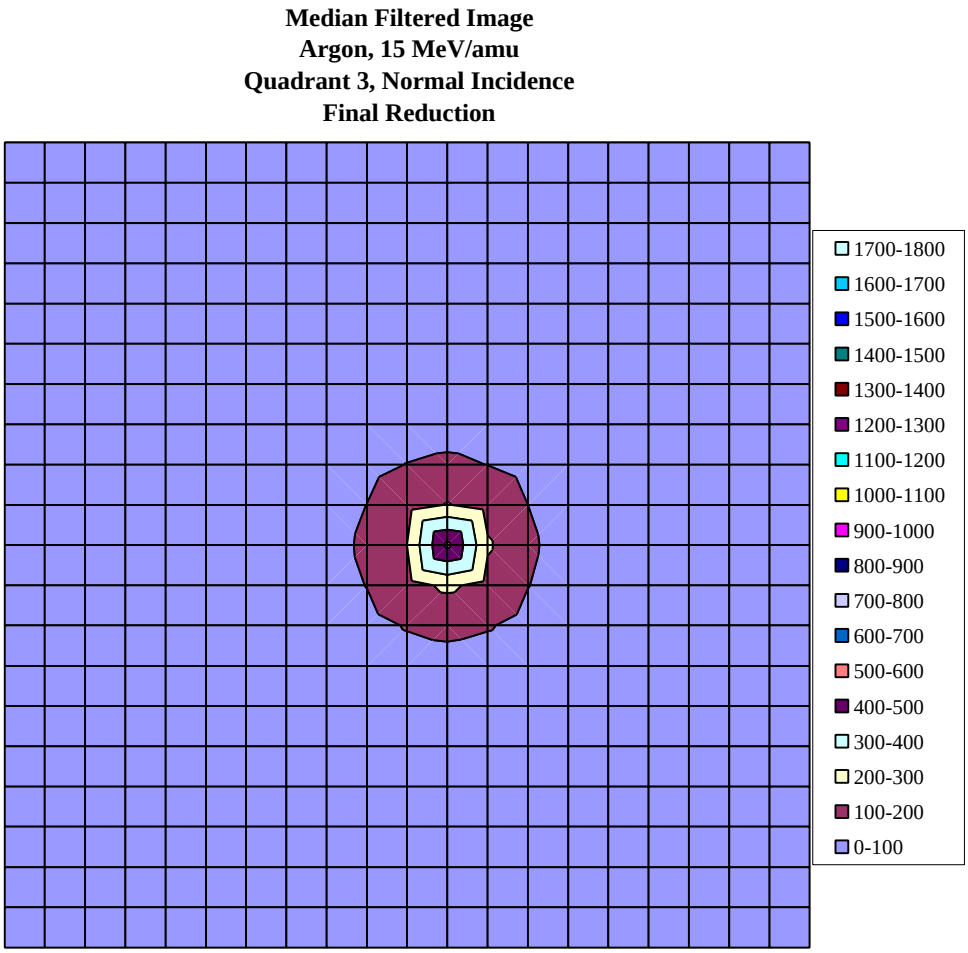

Figure E1. Quadrant 3 0º ion track. Signal is in counts.

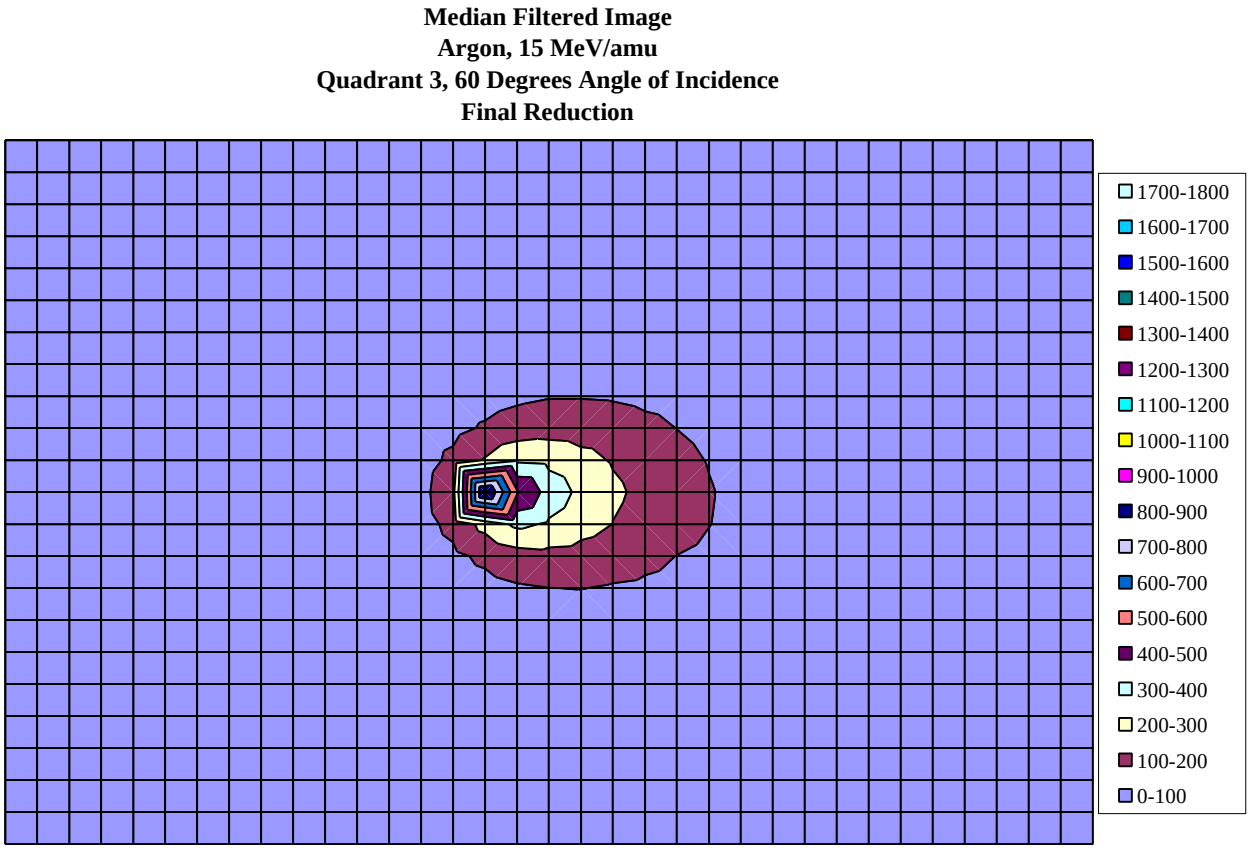

Figure E2. Quadrant 3 60º ion track. Signal is in counts.

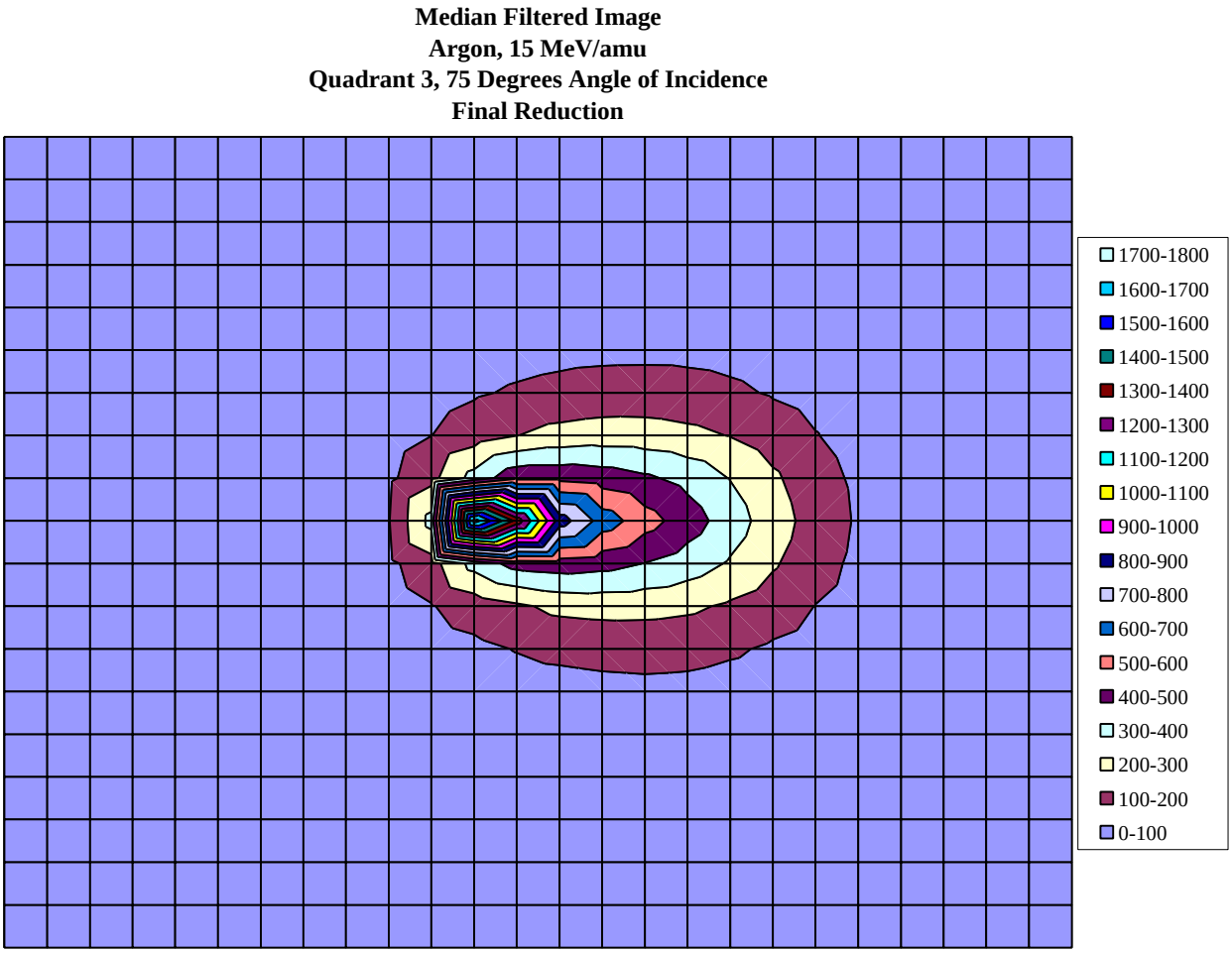

Figure E3. Quadrant 3 75º ion track. Signal is in counts.

Appendix F

Quadrant 4 Ion Track Contours

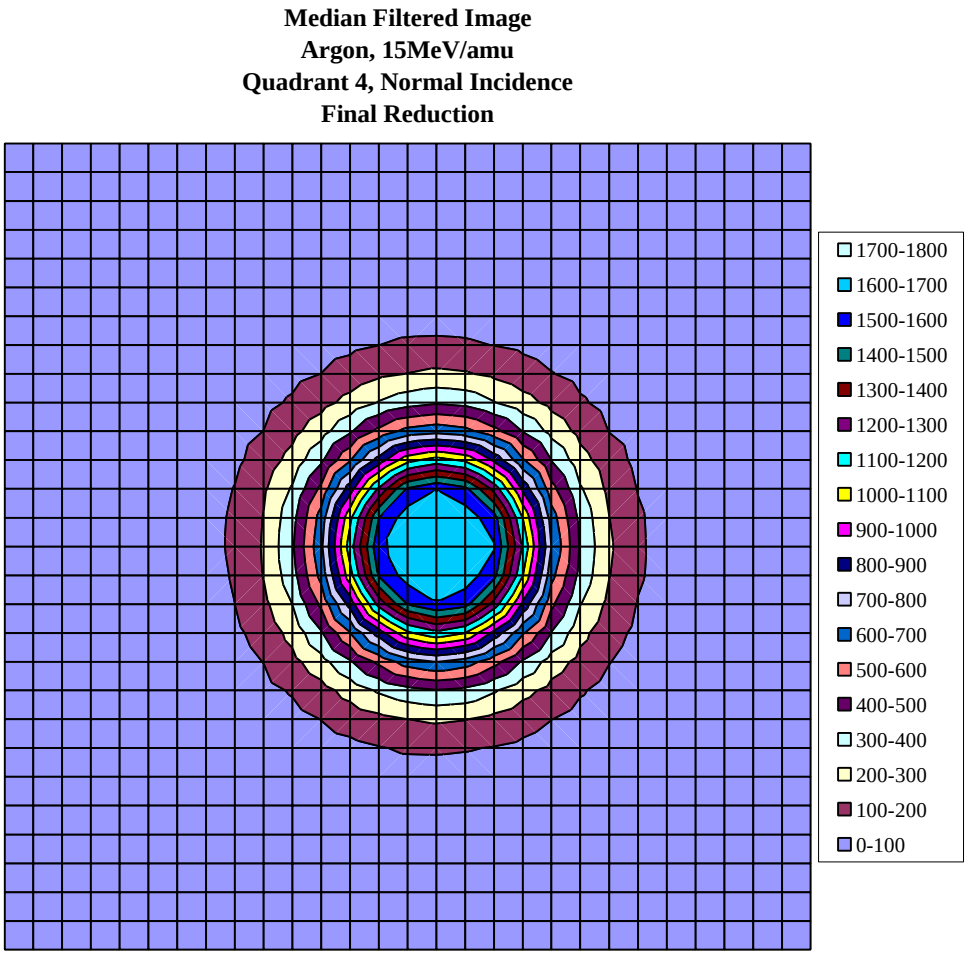

Figure F1. Quadrant 4 0º ion track. Signal is in counts.

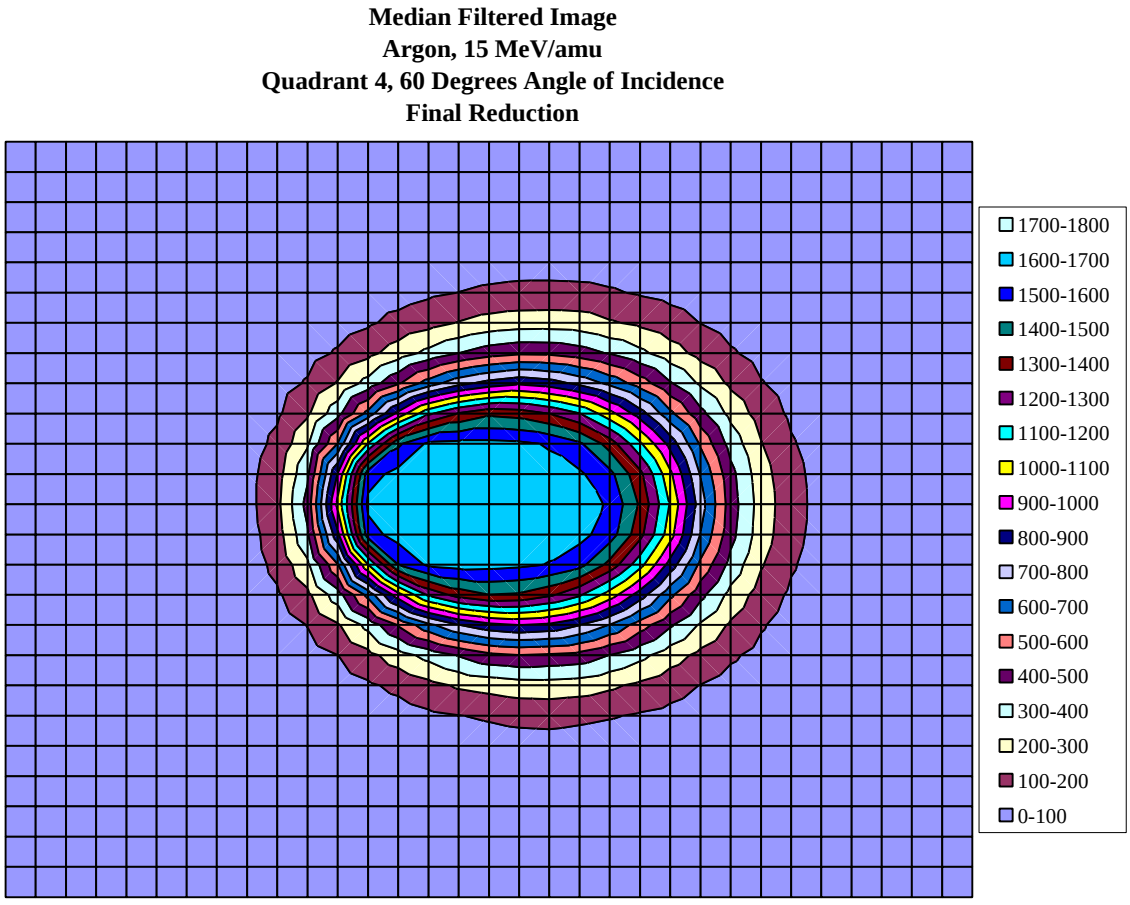

Figure F2. Quadrant 4 60º ion track. Signal is in counts.

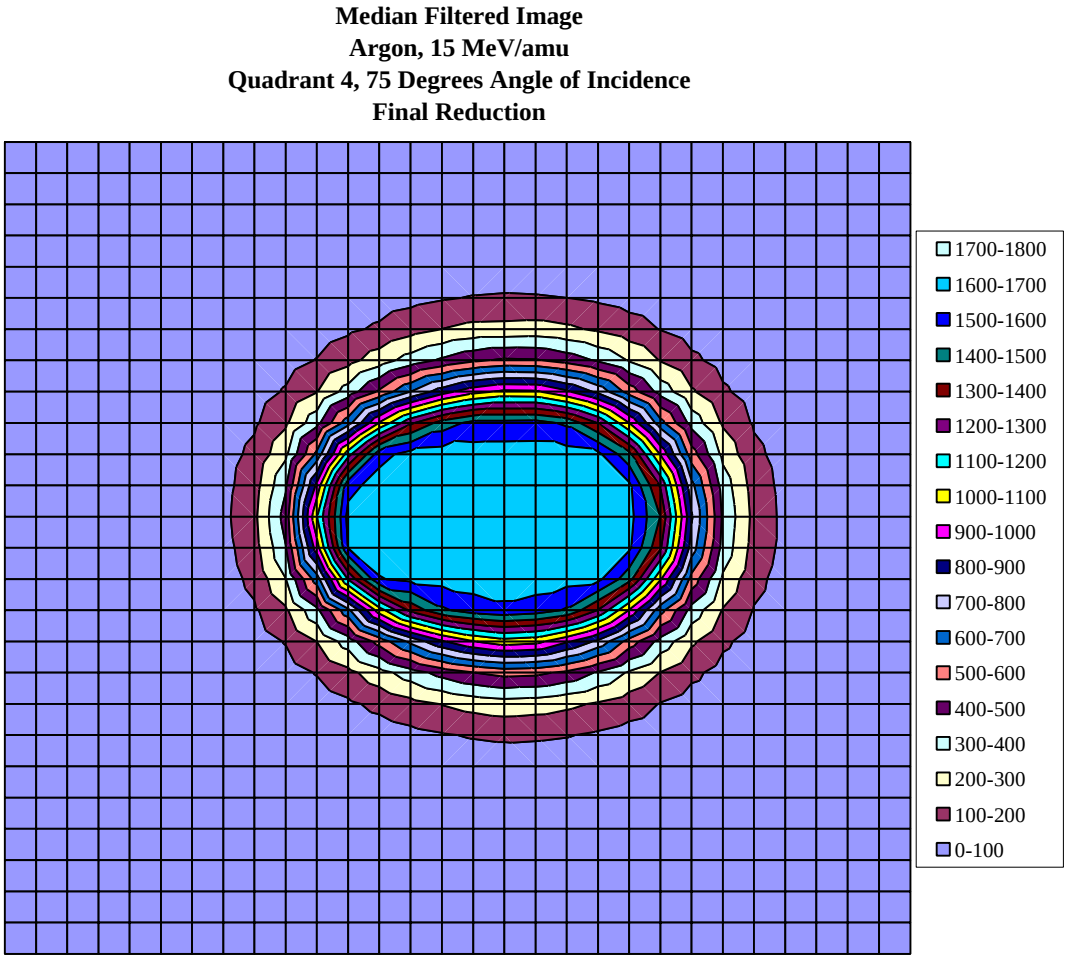

Figure F3. Quadrant 4 75º ion track. Signal is in counts.